Simulation of the crystallization process of Ge$_2$Sb$_2$Te$_5$ nanoconfined in superlattice geometries for phase change memories Supplementary Information

Debdipto Acharya, Omar Abou El Kheir, Simone Marcorini, and Marco

Bernasconi[*]

Department of Materials Science, University of Milano-Bicocca, Via R. Cozzi 55, I-20125

Milano, Italy

E-mail: marco.bernasconi@unimib.it

Table S1: Average coordination number for different pairs of atoms computed from the partial pair correlation functions for models of amorphous GST generated with and without (from Ref.[1]) vdW corrections, both at the experimental density of the amorphous phase of 0.0309 atom/$Å^3$ (bulk-LD). The theoretical results are compared with experimental data from anomalous x-ray scattering (AXS),[2] extended x-ray absorption spectroscopy (EXAFS),[3] and reverse Monte-Carlo (RMC) analysis of combined x-ray and neutron diffraction and EXAFS.[4] A more comprehensive comparison of experimental data with previous DFT calculations with PBE and other functionals is reported in a very recent work (see Table 5 in Ref.[5]). To determine the coordination numbers, we used 3.2 Å as a bond cutoff for all pairs except for Te-Sb for which we used 3.4 Å. In the experimental work of Ref.[4] they used as cutoff the first minimum of the pair correlation functions corresponding to (Ge-Ge) 3.05 Å, (Sb-Ge) 3.18 Å, (Te-Ge) 3.18 Å, (Sb-Sb) 3.28 Å, (Te-Te) 3.29 Å, and (Te-Sb) 3.35 Å. For the sake of comparison, we report in the last column the coordination numbers of our models computed with the cutoffs of Ref.[4] .

		NN	NN+vdW	AXS[2]	EXAFS[3]	RMC[4]	NN+vdW (cutoff of Ref.[4])
Ge	with Ge	0.33	0.33	0.7	0.6	0.69	0.31
	with Sb	0.30	0.33		0.0	0.83	0.30
	with Te	3.35	3.53	3.26	3.3	2.72	3.31
	Total	3.99	4.19	4.24	3.9	4.24	3.92
Sb	with Ge	0.30	0.33		0.0	0.83	0.30
	with Sb	0.55	0.51		0.0	0.00	0.58
	with Te	3.20	3.64	2.51	2.8	2.39	3.08
	Total	4.06	4.46	2.95	2.8	3.22	3.96
Te	with Ge	1.34	1.41	1.30	1.2	1.08	1.33
	with Sb	1.28	1.45	1.00	1.2	0.96	1.23
	with Te	0.31	0.29		0.0	0.00	0.37
	Total	2.93	3.16	2.30	2.4	2.04	2.93

Table S2: Position (Å) of the first maximum of the partial pair correlation functions for models of amorphous GST generated with and without (from Ref.[1]) vdW corrections, both at the experimental density of the amorphous phase of 0.0309 atom/$Å^3$ (bulk-LD). The theoretical results are compared with experimental data from anomalous x-ray scattering (AXS),[2] extended x-ray absorption spectroscopy (EXAFS),[3] and reverse Monte-Carlo (RMC) analysis of combined x-ray and neutron diffraction and EXAFS.[4] A more comprehensive comparison of experimental data with previous DFT calculations with PBE and other functionals is reported in a very recent work (see Table 5 in Ref.[5]).

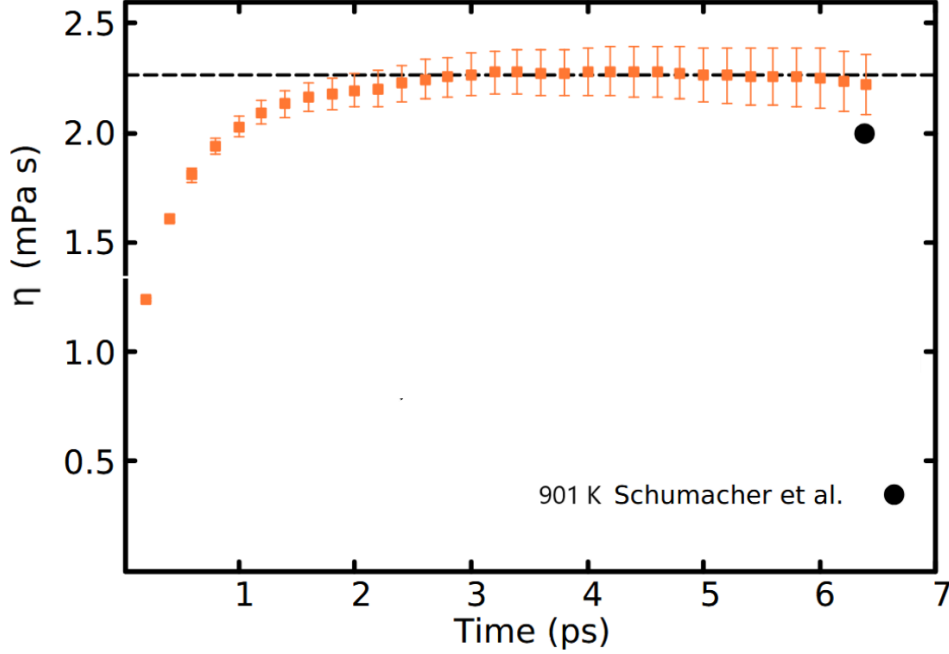|		NN	NN+vdW	AXS[2]	EXAFS[3]	RMC[4]
Ge	with Ge	2.62	2.61	2.50	2.47	2.48
	with Sb	2.82	2.80		2.69	
	with Te	2.78	2.76	2.65	2.63	2.64
Sb	with Sb	2.99	2.99			
	with Te	2.96	2.92	2.82	2.83	2.83
Te	with Te	3.04	2.95			

Figure S1: Viscosity η of GST at 900 K at the experimental density of the liquid. The value of $\eta(t)$ is shown as a function of the integration time t in the Green-Kubo formula $\eta = \lim_{t\to\infty} \frac{V}{k_B T} \int_0^t \langle \sigma_{xy}(t' + t_o)\sigma_{xy}(t_o)\rangle dt' = \lim_{t\to\infty} \eta(t)$, where V is the supercell volume, T is the temperature, and σ_{xy} is the off-diagonal component of the stress tensor. The average $\langle \ldots \rangle$ is over the initial times t_o. We also took an average over the three off-diagonal components xy, xz, and yz. In practice, η is evaluated from the plateau in the value of $\eta(t)$ at intermediate times, while at longer times the integral does not necessarily converge due to accumulation of noise.[6] We choose a maximum t_{max} to evaluate $\eta(t)$ equal to twice the time at which the correlation function $\langle \sigma_{xy}(t + t_o)\sigma_{xy}(t_o)\rangle$ goes to zero. We performed blocks averages by first averaging over t_o in $\langle \sigma_{xy}(t + t_o)\sigma_{xy}(t_o)\rangle$ in blocks with time length of $2t_{max}$. We then obtain the average $\eta(t)$ resulting from the Green-Kubo formula and its mean square errors by averaging over blocks. The resulting estimate of η from the plateau (dashed line) is η=2.3 $\pm$ 0.2 mPa·s to be compared with the experimental value of 2.0 mPa·s of Ref.[7]
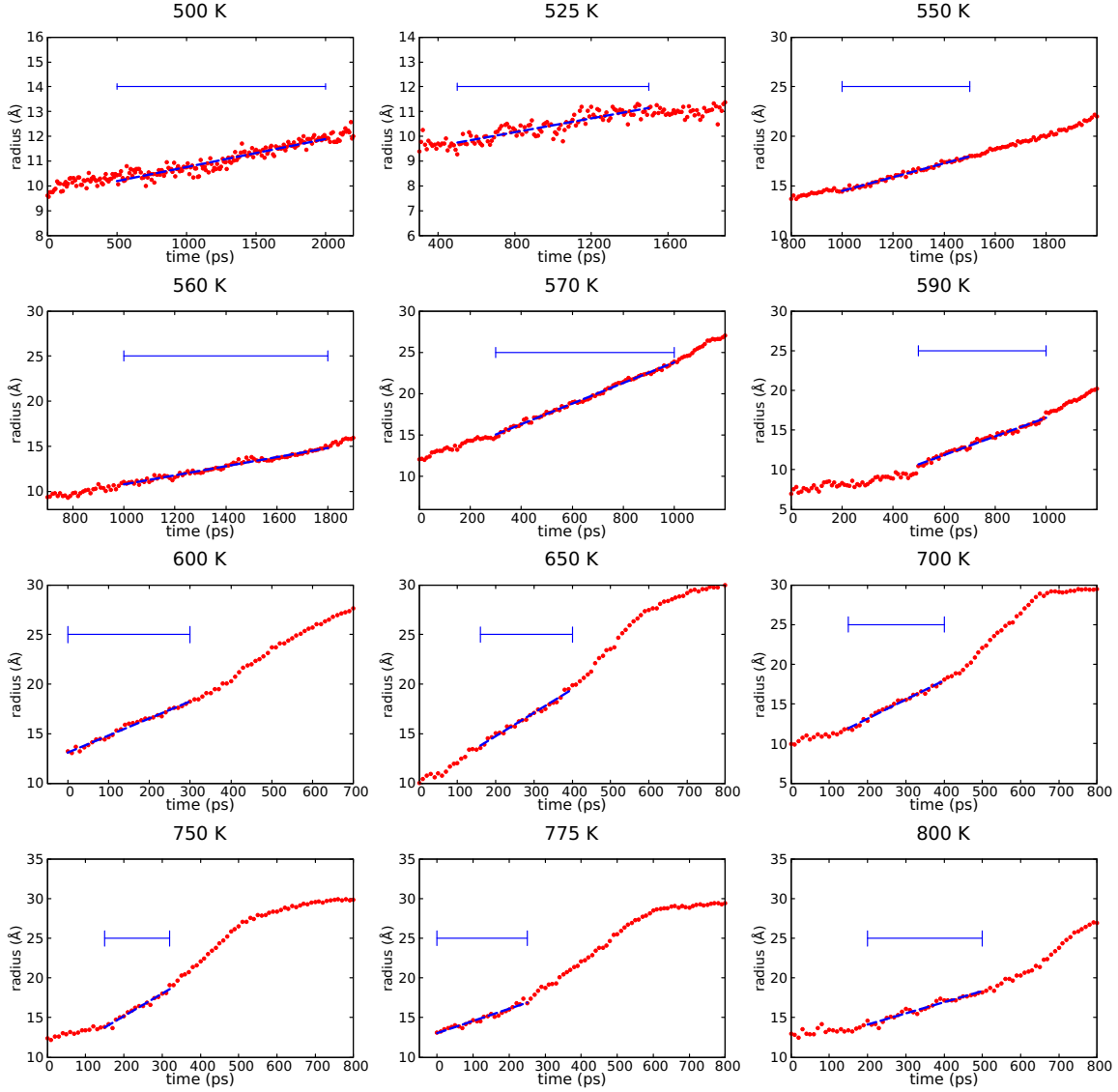
Figure S2: The evolution of the radius of the crystalline nuclei as a function of time in the NN+vdW simulations of the bulk at different temperatures and at the experimental density (bulk-LD). The linear fit in the range highlighted by horizontal bars yields the crystal growth velocity (see Table 3 in the article).
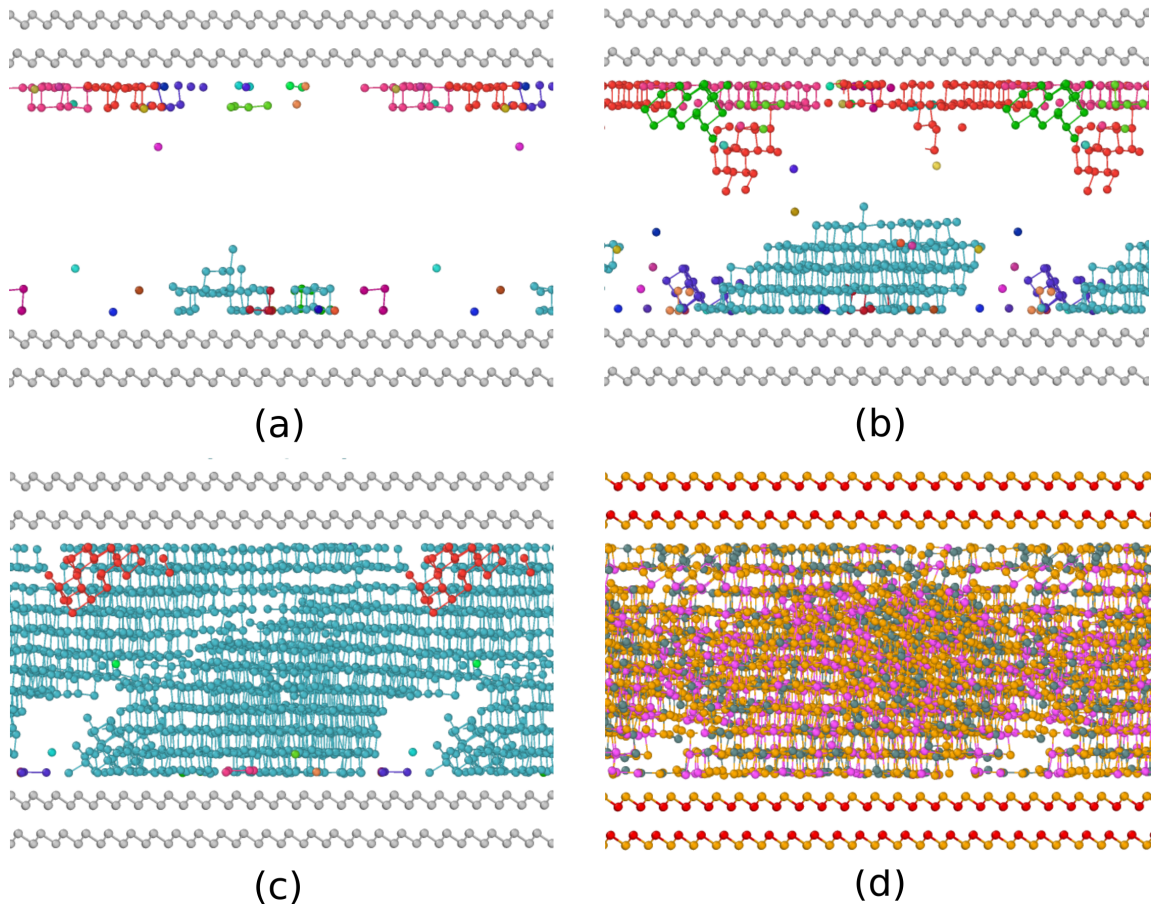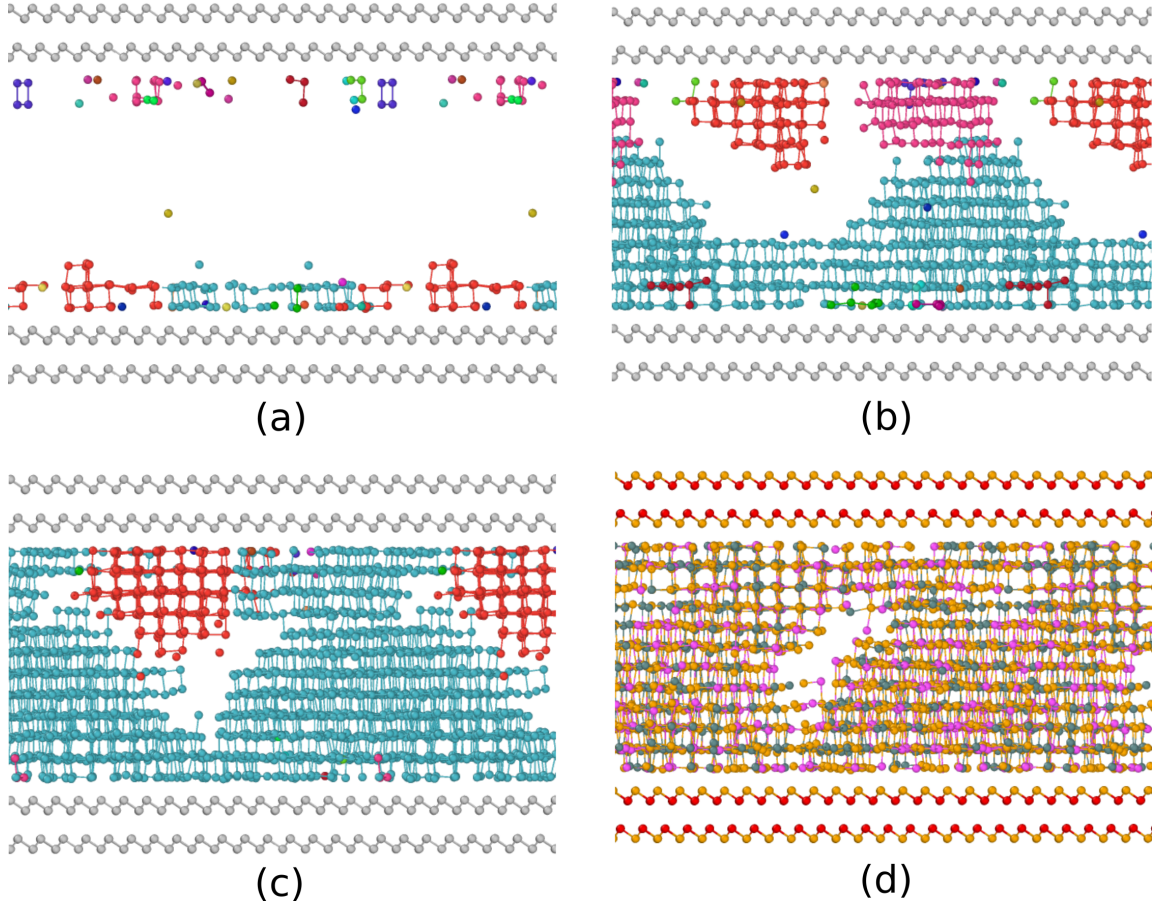
Figure S3: Simulation of the crystallization of a 3528-atom slab of amorphous GST capped by bilayers mimicking confinement by TiTe$_2$ in GST/TiTe$_2$-like SL (SL-HD). Snapshots at different times at 650 K are shown for (a) 0.5 ns, (b) 1 ns, and (c) 1.5 ns. Only crystalline atoms, identified by the Q_4^{dot} order parameter (see article), are shown. Different crystalline nuclei have different colors. (d) Final configuration after 2 ns. The color code is the same of Fig. 1 of the article.
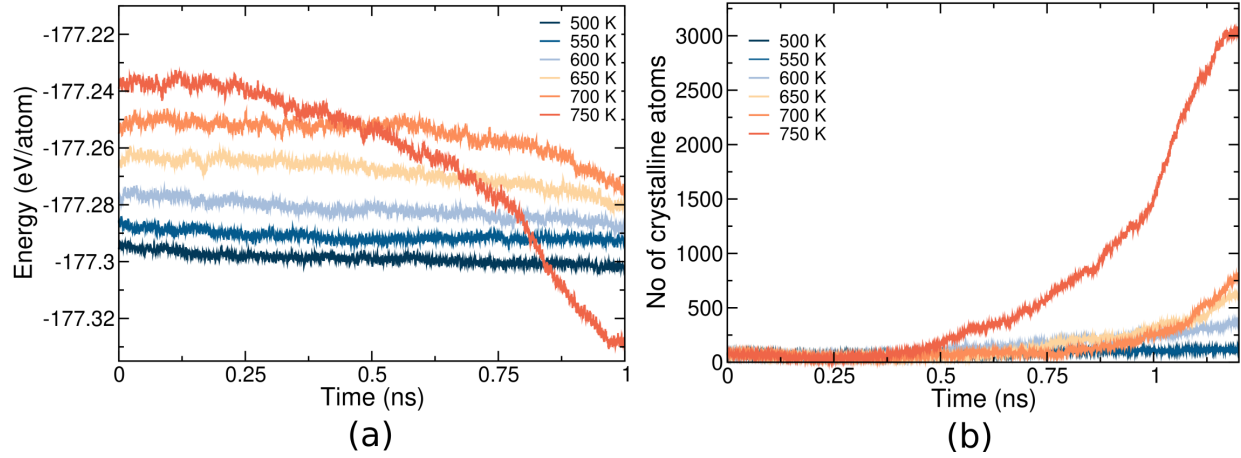
5

Figure S4: Simulation of the crystallization of a 3528-atom slab of amorphous GST capped by bilayers mimicking confinement by $TiTe_2$ in GST/$TiTe_2$-like SL (SL-HD). Snapshots at different times at 700 K are shown for (a) 0.5 ns, (b) 1 ns, and (c) 1.5 ns. Only crystalline atoms, identified by the Q_4^{dot} order parameter (see article), are shown. Different crystalline nuclei have different colors. (d) Final configuration after 2 ns. The color code is the same of Fig. 1 of the article.

Figure S5: Crystallization of amorphous GST capped by bilayers mimicking confinement by TiTe$_2$ in GST/TiTe$_2$ SL at lower density (SL-LD', see text) at different temperatures. (a) Potential energy and (b) number of crystalline atoms as a function of time.
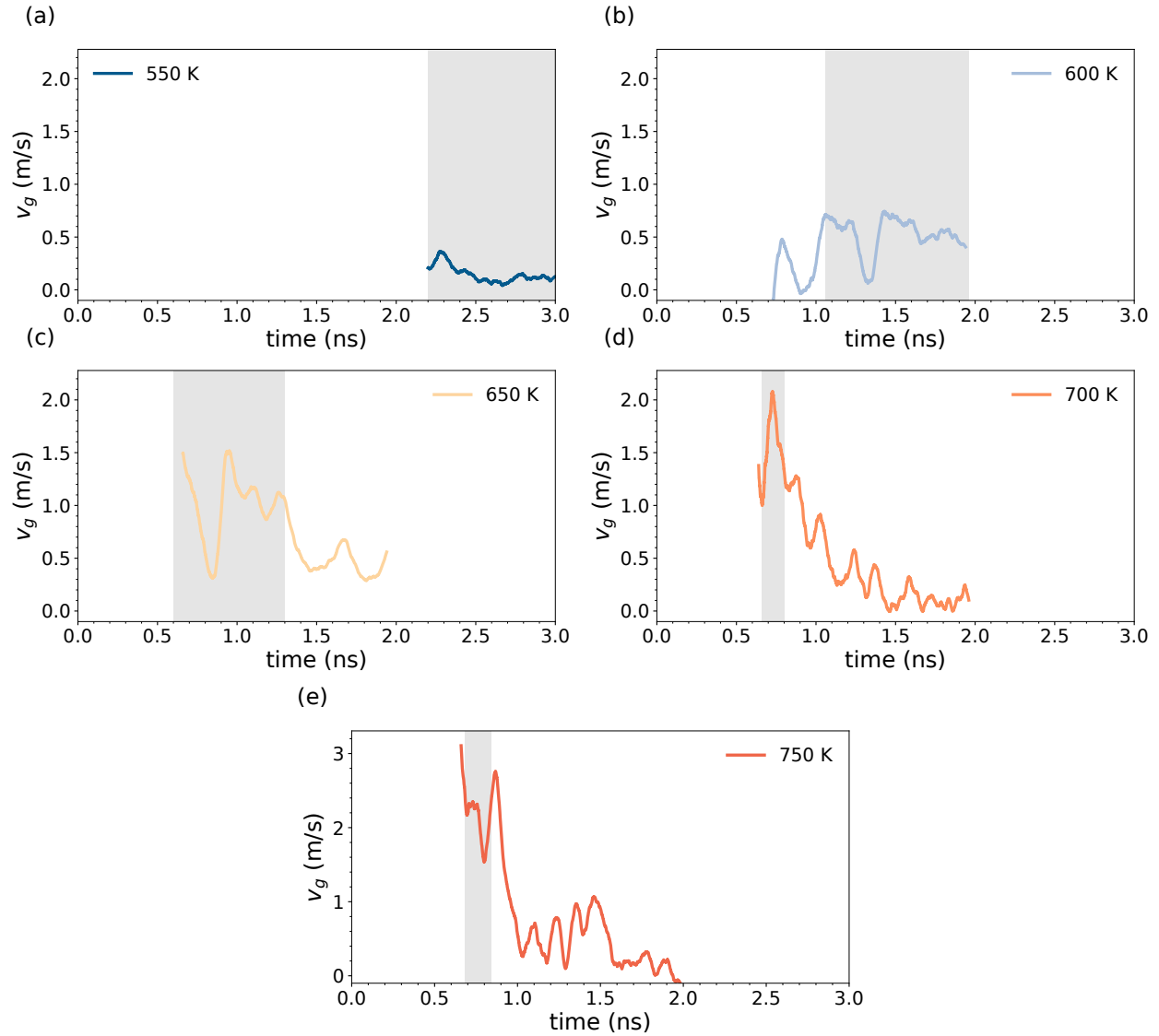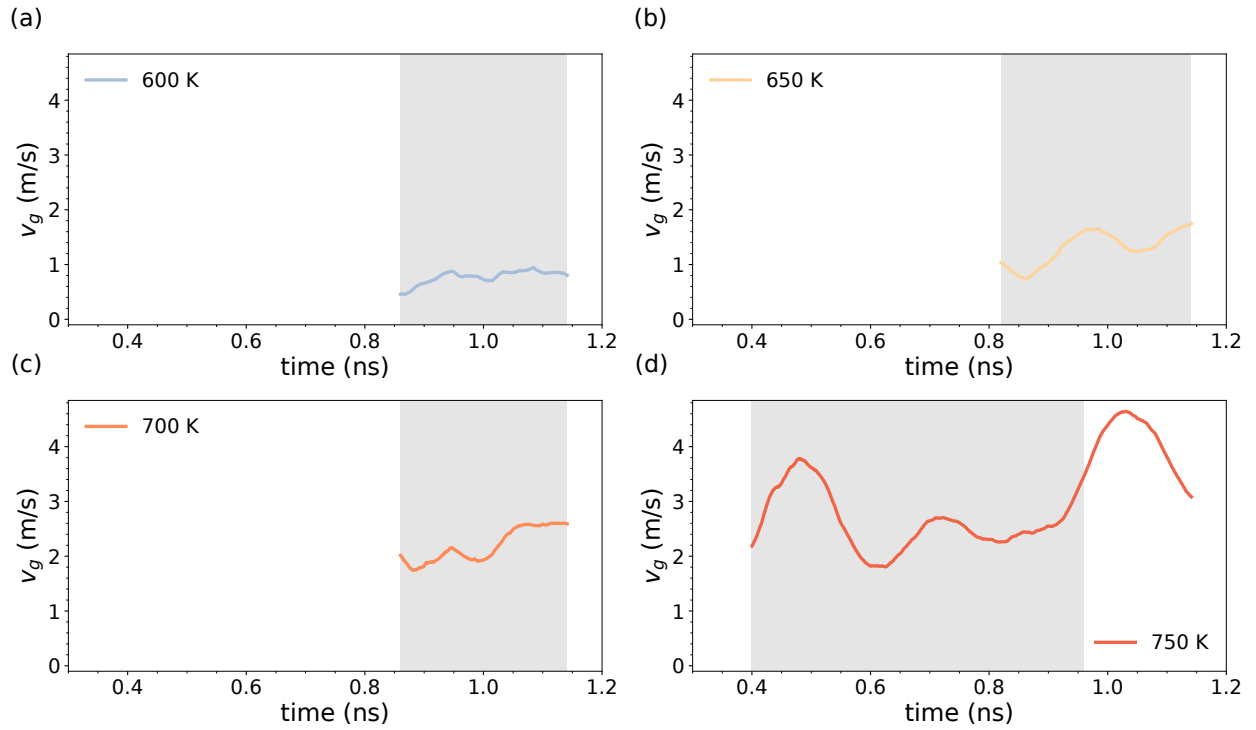
Figure S6: (a)-(e) Instantaneous crystal growth velocity (v_g) as a function of time at different temperatures for the SL-HD model. The region highlighted in gray corresponds to the time interval over which we estimated the average crystal growth velocities reported in Table 3 in the article.
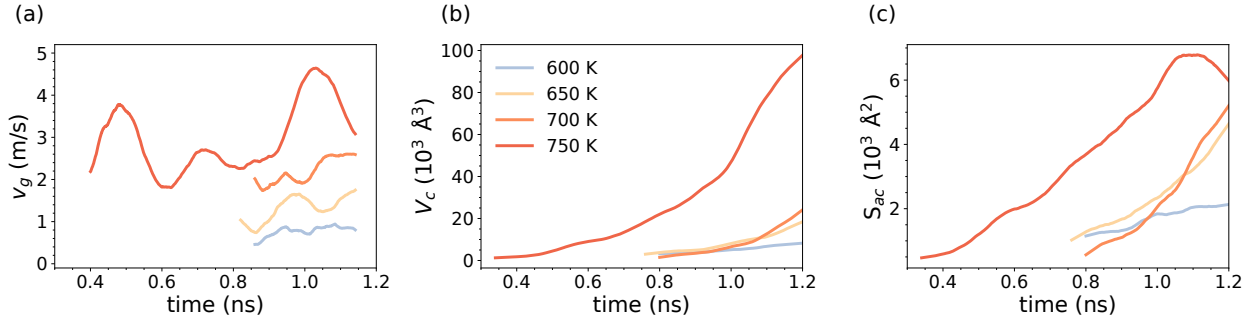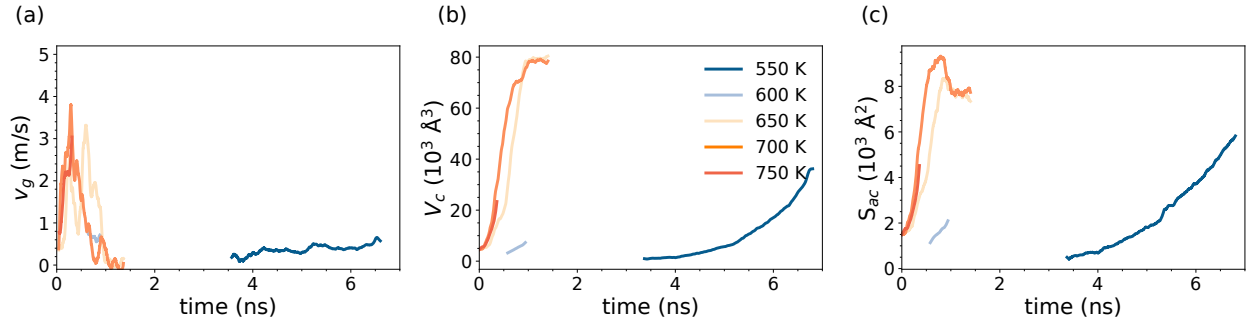
Figure S7: (a) Instantaneous crystal growth velocity v_g, (b) volume occupied by the crystalline atoms V_c and (c) area of the crystal-amorphous interface S_{ac} as a function of time at the different temperatures for the SL-LD' model.

Figure S8: (a)-(d) Instantaneous crystal growth velocity (v_g) as a function of time at different temperatures for the SL-LD' model. The region highlighted in gray corresponds to the time interval over which we estimated the average crystal growth velocities reported in Table 3 in the article.

9

Figure S9: (a) Instantaneous crystal growth velocity v_g, (b) volume occupied by the crystalline atoms V_c and (c) area of the crystal-amorphous interface S_{ac} as a function of time at the different temperatures for the bulk simulations at low density (bulk-LD).
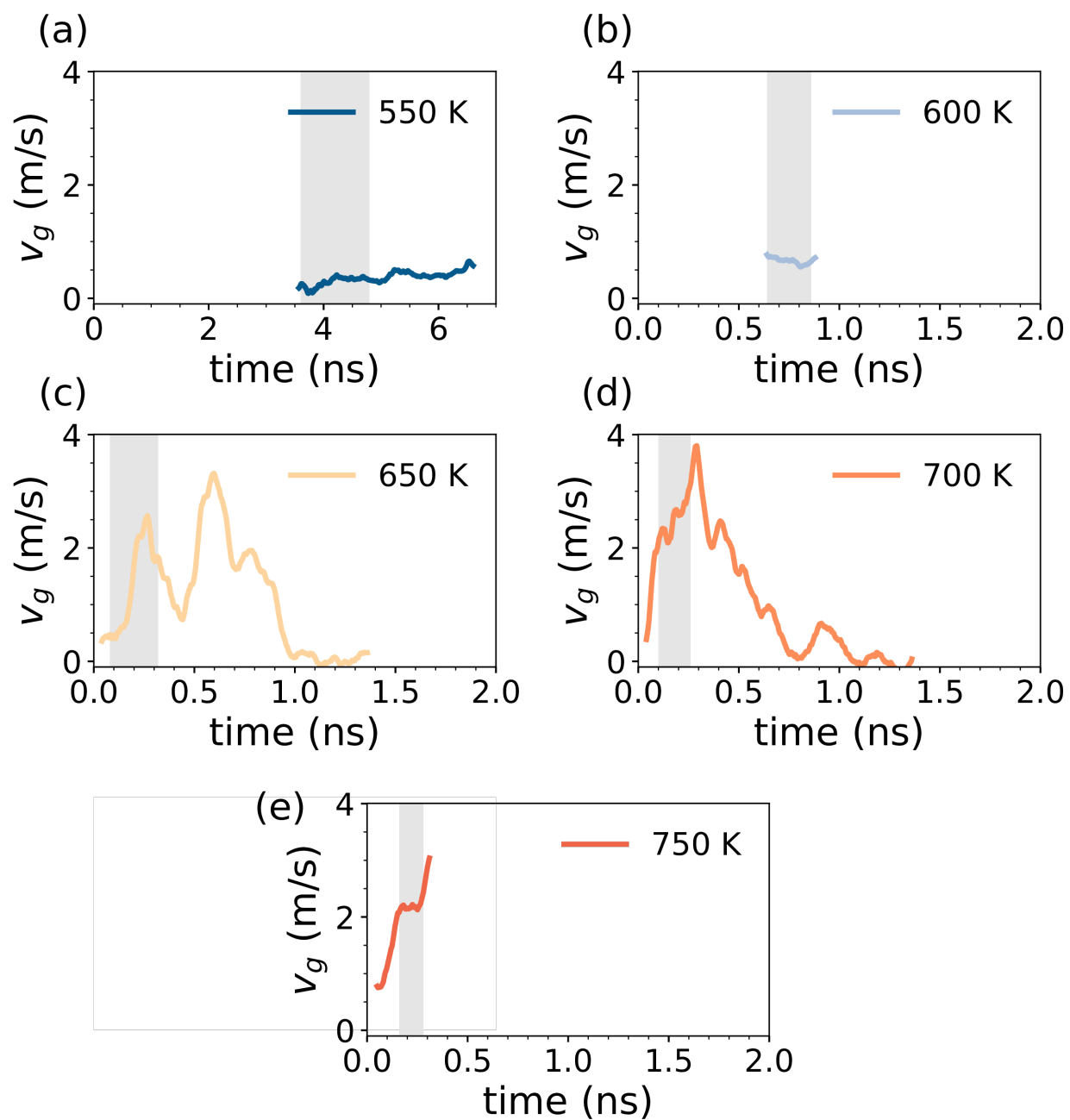
Figure S 10: (a)-(e) Instantaneous crystal growth velocity (v_g) as a function of time at different temperatures for the bulk at low density (bulk-LD). The region highlighted in gray corresponds to the time interval over which we estimated the average crystal growth velocities reported in Table 3 in the article.
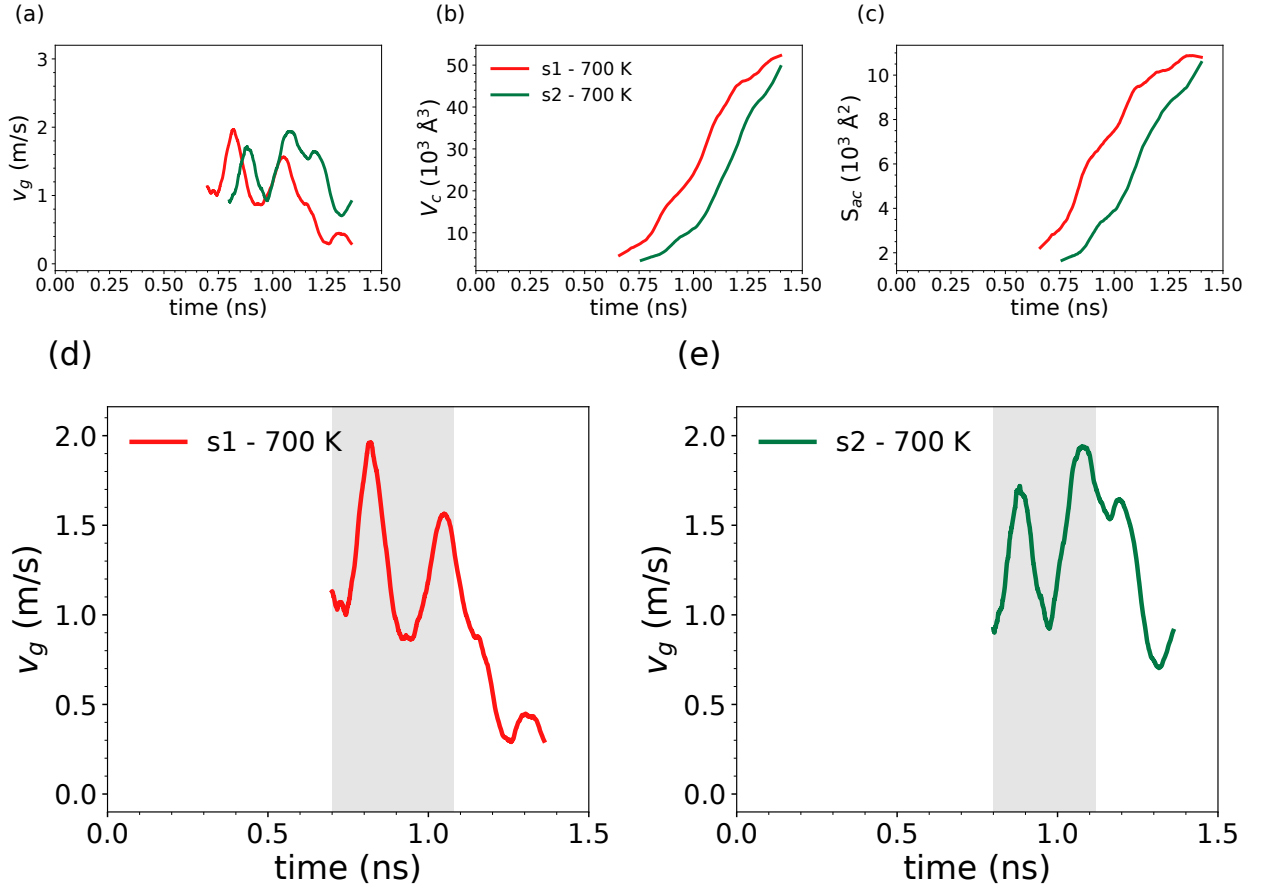
Figure S11: (a) Instantaneous crystal growth velocity v_g, (b) volume occupied by the crystalline atoms V_c, (c) area of the crystal-amorphous interface S_{ac} as a function of time at 700 K in other two independent models for the SL-HD geometry. (d)-(e) Instantaneous crystal growth velocity (v_g) as a function of time where region highlighted in gray corresponds to the time interval over which we estimated the average crystal growth velocities reported in Table 3 in the article.
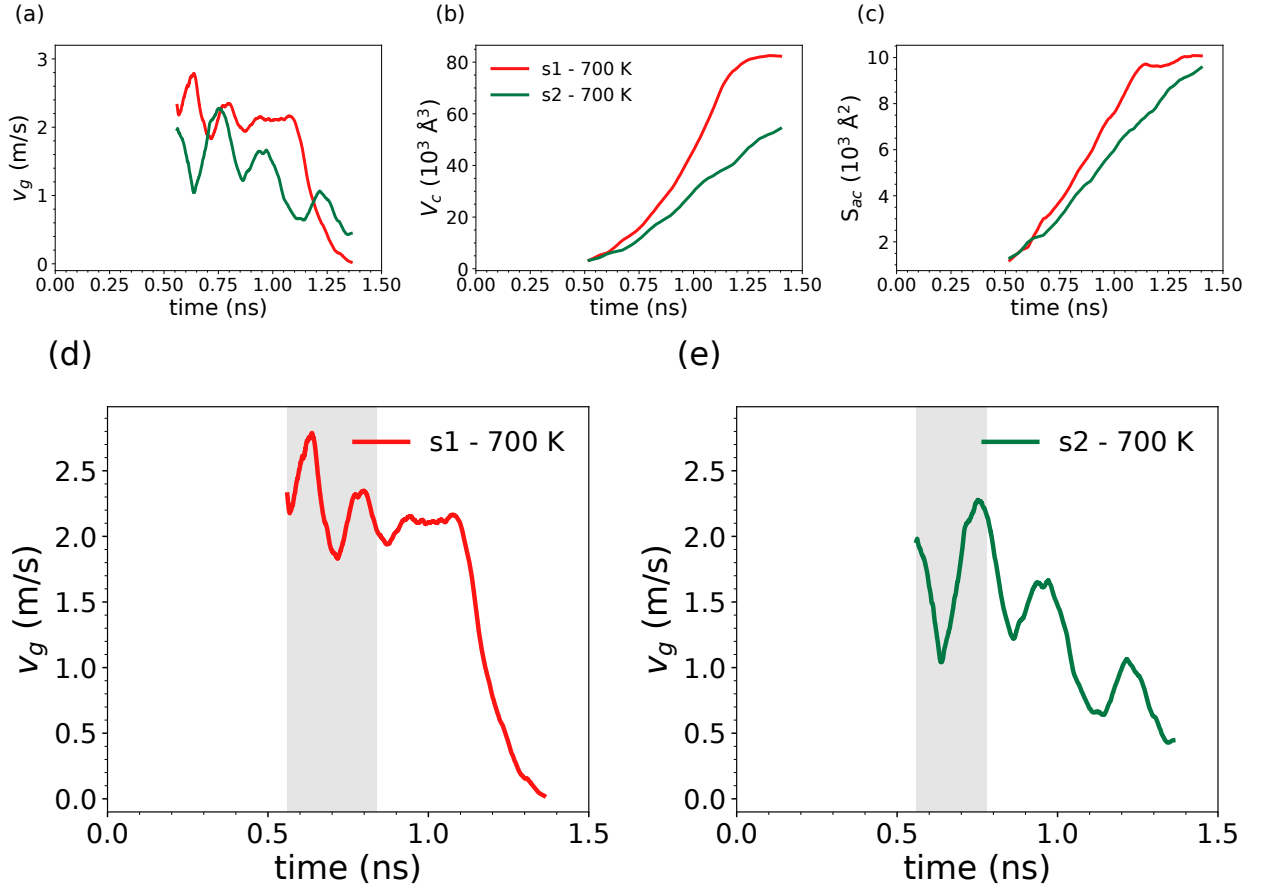
Figure S12: (a) Instantaneous crystal growth velocity v_g, (b) volume occupied by the crystalline atoms V_c, (c) area of the crystal-amorphous interface S_{ac} as a function of time at 700 K in other two independent models of the SL-LD' geometry. (d)-(e) Instantaneous crystal growth velocity (v_g) as a function of time where region highlighted in gray corresponds to the time interval over which we estimated the average crystal growth velocities reported in Table 3 in the article.

Table S3: Two-dimensional diffusion coefficient D as a function of time of the SL at the equilibrium density of the hexagonal phase (SL-HD, see article), from NVE simulations at the average temperatures given in the first column. We computed D from the two dimensional mean square displacement (MSD) in the plane perpendicular to the slab thickness in the SL as $<x^2> + <y^2> = 4Dt$. The diffusion coefficient in the slab is compared to those in the bulk at the same density (bulk-HD, see article) at the average temperatures given in the third column. The calculations refer to amorphous models equilibrated at 300 K and then heated and equilibrated at the target temperature in 100 ps. D was then computed in the subsequent NVE simulations lasting 400 ps.

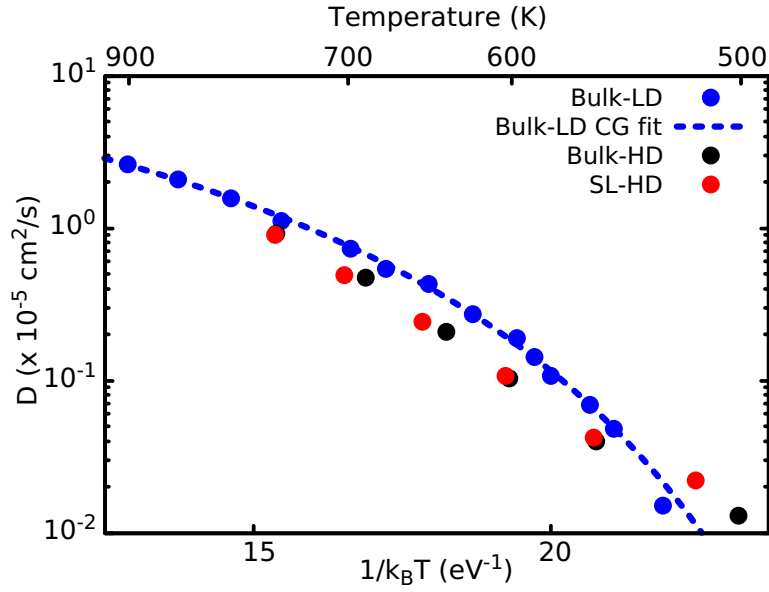| Temperature (K)	D (10^{-6}cm^2/s) SL-HD	Temperature (K)	D (10^{-6}cm^2/s) Bulk-HD
517	0.22	501	0.13
560	0.42	559	0.40
603	1.07	601	1.04
651	2.44	636	2.08
702	4.90	687	4.69
756	8.99	755	9.13

Figure S13: Diffusion coefficient D (10^{-5} cm^2/s) as a function of temperature from bulk NN+vdW simulations at the experimental density of the amorphous phase (bulk-LD) and of the crystalline hexagonal phase (bulk-HD) and of the superlattice model SL-HD (see article).
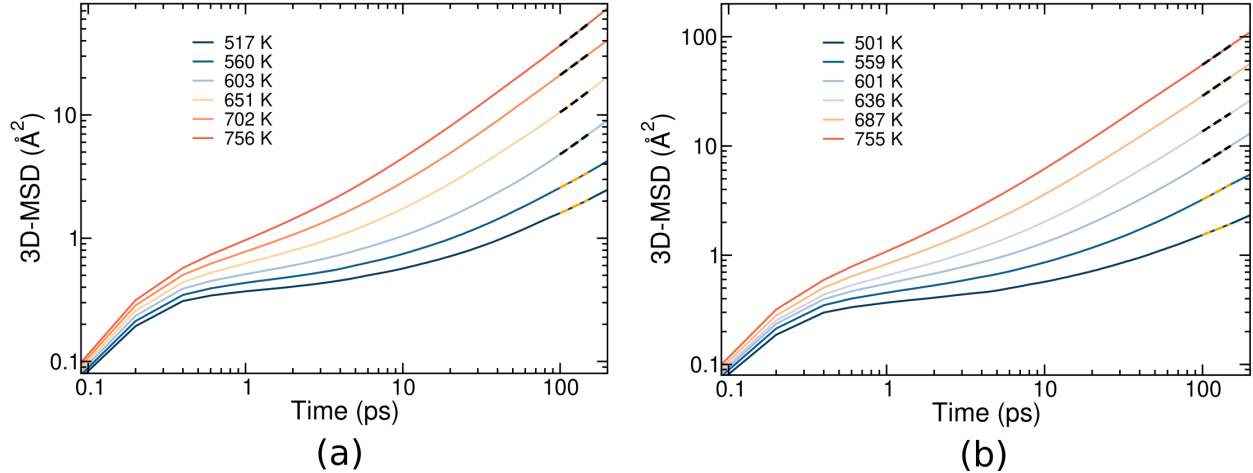
Figure S14: Mean square displacement (MSD) as a function of time from NVE simulations at the average temperatures given in the inset for (a) SL at the equilibrium density of the hexagonal phase (SL-HD) and (b) for the bulk at the same density (bulk-HD, see article). For the sake of comparison with the bulk, the 3D-MSD is plotted for the SL as well, where 3D-MSD= $3/2(<x^2> + <y^2>)$.

References

(1) Abou El Kheir, O.; Bonati, L.; Parrinello, M.; Bernasconi, M. Unraveling the crystallization kinetics of the $Ge_2Sb_2Te_5$ phase change compound with a machine-learned interatomic potential. *npj Comput. Mater.* **2024**, *10*, 33.

(2) Stellhorn, J. R.; Hosokawa, S.; Kohara, S. Local- and Intermediate-Range Structures on Ordinary and Exotic Phase-Change Materials by Anomalous X-ray Scattering. *Anal. Sci.* **2020**, *36*, 5–9.

(3) Baker, D. A.; Paesler, M. A.; Lucovsky, G.; Agarwal, S. C.; Taylor, P. C. Application of Bond Constraint Theory to the Switchable Optical Memory Material $Ge_2Sb_2Te_5$. *Phys. Rev. Lett.* **2006**, *96*, 255501.

(4) Jóvári, P.; Kaban, L.; Steiner, J.; Beuneu, B.; Schöps, A.; Webb, A. 'Wrong bonds' in sputtered amorphous $Ge_2Sb_2Te_5$. *J Phys.: Condens. Matter* **2007**, *19*, 335212.

(5) Pethes, I.; Piarristeguy, A.; Pradel, A.; Michalik, J., S. Darpentigny; Zitolo, A.; Escalier, R.; Jóvári, P. Short-range order and topology of Te-rich amorphous Ge–Sb–Te alloys. *J. Amer. Ceramic Soc.* **2025**, *108*, e20258.

(6) Yong, Z.; Otani, A.; Maginn, E. J. Reliable Viscosity Calculation from Equilibrium Molecular Dynamics Simulations: A Time Decomposition Method. *J. Chem. Theory Comput.* **2015**, *11*, 3537–3546.

(7) Schumacher, M.; Weber, H.; Jóvári, P.; Tsuchiya, Y.; Youngs, T. G.; Kaban, I.; Mazzarello, R. Structural, electronic and kinetic properties of the phase-change material $Ge_2Sb_2Te_5$ in the liquid state. *Sci. Rep.* **2016**, *6*, 27434.